

**THIS DOCUMENT IS PART OF A NEW BOOK, IT IS BROUGHT TO YOU FREELY BY THE OPEN ACCESS JOURNAL MATERIALS AND DEVICES**

<http://materialsanddevices.co-ac.com>

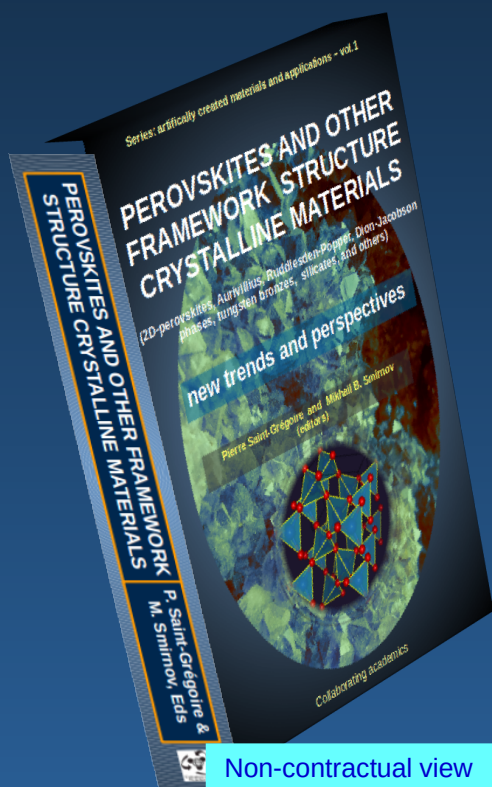
**The book,  
“PEROVSKITES AND OTHER FRAMEWORK  
STRUCTURE MATERIALS**

(2D-perovskites, Aurivillius, Ruddlesden-Popper, Dion-Jacobson phases, tungsten bronzes, clays, and others)

**New trends and perspectives”**

(editors P. Saint-Grégoire and M.B Smirnov)

Is a collective volume of 800 pages with **76 authors** and **26 chapters** on recent developments and hot subjects, divided into two parts:



**A. Fundamental aspects and general properties**

**B. Elaborated materials and applied properties**

Available in 3 formats:

- Ebook
- printed softcover, black & white
- printed hardcover, color.



**Go to the Book(click)**

Non-contractual view



---

## ***Chap. 21 : Experimental methods to study clay minerals and perspective applications of Fluorohectorite***

---

P. H. Michels-Brito (1), L. Michels (1), K. W. B. Hunvik (1), E.C. dos Santos (1,2), B. Pacáková (1), L. P. Cavalcanti (1,3), K. D. Knudsen (1,3), H. N. Bordallo (2,4) and J. O. Fossum (1)

(1) Department of Physics, Norwegian University of Science and Technology (NTNU), Trondheim, Norway

(2) Niels Bohr Institute (NBI), University of Copenhagen, Copenhagen, Denmark

(3) Physics Department, Institute for Energy Technology (IFE), P.O. Box 40, N-2027 Kjeller, Norway

(4) European Spallation Source, Lund, Sweden

Corresponding authors : [jon.fossum@ntnu.no](mailto:jon.fossum@ntnu.no) and [bordallo@nbi.ku.dk](mailto:bordallo@nbi.ku.dk)

---

**Abstract** : Fluorohectorite is a synthetic 2:1 layer smectite clay where the presence of exchangeable cations located between water molecules in the interlayer space allows for expansion of the crystal lattice. This swelling property is extremely relevant to many applications including water treatment, bioactive molecules intercalation (drug delivery), soil remediation, CO<sub>2</sub> capture as well as extra-terrestrial environment studies. In the present chapter, the aim is to discuss why Fluorohectorite can be in particular advantageous for many applications where retention of big volumes is an issue. We will also discuss on the main experimental techniques used to study these materials.

**Keywords** : CLAY MINERALS, FLUOROHECTORITE, INTERCALATION, ECOMATERIALS, NANOMATERIALS, BIOMOLECULES ENCAPSULATION, GAS ADSORPTION, LOW COST MATERIAL

**Cite this paper:** P. H. Michels-Brito, L. Michels, K. W. B. Hunvik, E.C. dos Santos, B. Pacáková, L. P. Cavalcanti, K. D. Knudsen, H. N. Bordallo and J. O. Fossum, OAJ Materials and Devices, Vol. 5(2) (2021) - chap No21, p 601 in "Perovskites and other framework structure crystalline materials: new trends and perspectives" DOI:10.23647/ca.md20201501

---

## I. Introduction

Clay minerals are nano-lamellar materials formed by stacked nano-layers that consist of tetrahedral and octahedral sheets. Each tetrahedron in the layer is made up of a central cation, most commonly  $\text{Si}^{4+}$ ,  $\text{Al}^{3+}$  and  $\text{Fe}^{3+}$ , coordinated to four oxygen atoms linked to neighboring tetrahedra by sharing three basal oxygen atoms. The apical oxygen is located at a plane connecting the tetrahedron with an octahedral sheet. The octahedral sheet has a central cation - e.g.  $\text{Al}^{3+}$ ,  $\text{Fe}^{3+}$  or  $\text{Mg}^{2+}$  being the most common, nonetheless other cations, i.e.  $\text{Li}^+$ ,  $\text{Mn}^{2+}$ ,  $\text{Co}^+$ ,  $\text{Ni}^{2+}$ ,  $\text{Cu}^{2+}$ , can also partially substitute the cation - coordinated with the apical oxygen and also with a hydroxyl group. A clay layer can consist of one tetrahedral and one octahedral sheet (dioctahedral or trioctahedral 1:1 type) or of one octahedral sheet sandwiched between two tetrahedral sheets (dioctahedral or trioctahedral 2:1 type), Figure 1.

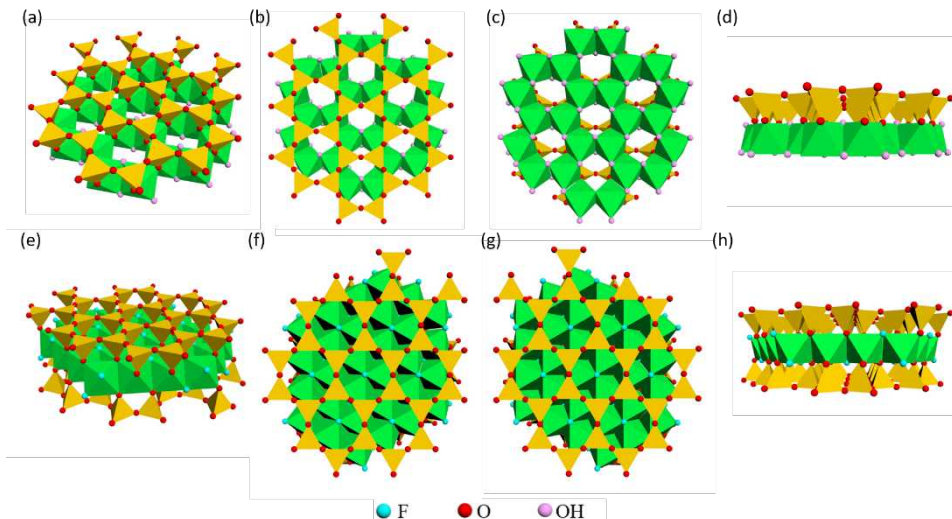


**Figure 1: Schematic structure of various clay minerals drawn using Autodesk 3ds Max 2020. Upper row: Kaolin (Kaol) type (a) dioctahedral 3D view, (b) dioctahedral top view, (c) dioctahedral bottom view, (d) dioctahedral side view. Lower row: Fluorohectorite (Fht) (e) trioctahedral 3D view, (f) trioctahedral top view, (g) trioctahedral bottom view and (h) trioctahedral side view.**

The dioctahedral 1:1 clay minerals (constituting the Kaolin group, hereafter K-group), have the general composition of  $\text{Al}_2\text{Si}_2\text{O}_5(\text{OH})_4$ . K-clay minerals show a wide variety of ordered and disordered polytypes, kaolinite [Kao], dickite, nacrite and halloysite [Hal] (containing water molecules within the interlayers), including stacking faults or defects occurring within the layers. The bonding between the K-layers is due to hydrogen bonding involving hydrogen atoms of one layer and the basal oxygen atoms of the adjacent layer <sup>[1]</sup>. This tight hydrogen bonding restricts expansion and limits the reactive area to external surfaces. As such, soils dominated by 1:1 mineral have low capacity for adsorbing cations and consequently low fertility. However, its inert chemical nature and its unique size, shape and structure makes the K-group important in applications such as filler in the plastics and paper industries, and it is also important in refractory applications, as catalysts, in concrete, in fiberglass, and as adsorbent for removal of organic compounds <sup>[2]</sup>.

The 2:1 clay minerals are represented by the mica, smectite [Sm], and vermiculite groups, as well as by the nonexpanding layer silicates talc and pyrophyllite. True micas have a similar structure to that of talc and pyrophyllite, in which the interlayer cation forms a strong bond between tetrahedral sheets in adjoining layers, consequently representing a limiting factor in the expansion of the mineral. Expandable 2:1 clay minerals, Sm, hectorite [Ht] and vermiculite, have similar layer structure to that of mica, and for these minerals the possibility of introduction of weakly bound cations, water, or polar organic molecules in the interlayer regions causes variations of interlayer spacing <sup>[3]</sup>. Montmorillonite [Mt], (i.e. bentonite [Bent]), the most common member of the Sm-group, has general molecular formula  $\text{M}_{0.33}\text{Al}_{1.67}(\text{Fe}^{2+}, \text{Mg}^{2+})_{0.33}\text{Si}_4\text{O}_{10}(\text{OH})_2(n\cdot\text{H}_2\text{O})$ , where M is the interlayer charge compensating cation (e.g. normally alkaline ( $\text{Li}^+$ ,  $\text{Na}^+$ ,  $\text{K}^+$ , ...)) or alkaline-earth cations ( $\text{Be}^{2+}$ ,  $\text{Mg}^{2+}$ ,  $\text{Ca}^{2+}$ , ...)) and  $n$  denotes the number of water molecules in the hydrated clay. This molecular formula displays one characteristic of Sm-clays, namely that there is considerable metallic substitution in the octahedral sheet. In the case of Mt,  $\text{Al}^{3+}$  is replaced by  $\text{Fe}^{2+}$  or  $\text{Mg}^{2+}$ . This substitution gives rise to a charge imbalance that is compensated by the interlayer cation  $\text{M}^+$ . The different Sm-groups have characteristic types of metallic substitutions in the octahedral positions <sup>[4]</sup>. The 2:1 layers in Sm are held together by van der Waals bonds and intercalated cation linkages, and for certain Sm such as Mt, this can comprise a weak enough bonding to allow for the swelling of the stack, i.e. expansion the crystal lattice in the **c**-direction upon exposure to

certain gases (such as water vapor) or liquids (such as liquid water). This crystalline swelling at low water exposure is step-wise and entails an integral number ( $n = 1, 2, 3$ ) of intercalated water layers (WL). At increased water exposure, the swelling process becomes osmotic, the layers delaminate, and a suspension of repulsive clay layers is formed, which depending on clay concentration may gel <sup>[5]</sup>. Alternatively, to e.g. Mt, a strong bonding of the interlayer cations holding the 2:1 layers together such as in general for vermiculite or illite [I], limits the expansion of the basal spacing and hinders osmotic swelling. Sm-minerals are widely applied as adsorbents, adhesives, animal feed bonds, nuclear waste barrier, catalysts, cement binder, cosmetics, emulsion stabilizer, food additives, pharmaceuticals, to name a few of the applications <sup>[6]</sup>.

The existence of charge in clay minerals, which can be structural (permanent charge) and surface charge (which usually depends on the value of pH, when in a suspension, and contributions from the edges of the sheets), is the basis for the two important properties in clay minerals, namely the cation exchange capacity (CEC) and the swelling properties. CEC is a measure of the capacity of clay minerals to exchange cations from the solution as well as a measure of the concentration of unfixed cations in the interlayers and surface layers, which depends on the magnitude of the total layer charge. Since the surface layer charge is the function of pH, thus, CEC also varies with pH. Usually CEC is measured at pH 7 <sup>[7]</sup>. CEC values of several clays are given in Table 1.

The common metallic cations found in exchange positions in clay minerals are  $\text{Ca}^{2+}$ ,  $\text{Mg}^{2+}$ ,  $\text{Na}^+$  and  $\text{K}^+$ . The swelling properties of Sm clay minerals are relevant to many existing or potential applications including environmental such as for  $\text{CO}_2$  capture/retention/transport, capture of/controlled delivery of certain drugs, as barriers for nuclear waste or chemical waste storage, for borehole stability in drilling operations, and additives for numerous industrial processes and commercial products (paints, cosmetics, certain foods, household products, production of polymer nanocomposites, etc) <sup>[8]</sup>.

**Table 1 : Cation exchange capacity (CEC) values of selected clays** <sup>[8, 9, 10, 11, 12]</sup>

Clay Mineral	CEC, meq/100 g
Allophane	70
Kaolinite [Kaol]	3-15
Halloysite [Hal]	5-10
Na -Montmorillonite [Na-Mt]	80-130
Ca - Montmorillonite [Ca-Mt]	40-70
Hectorite [Ht]	80-130
Synthetic Na <sub>x</sub> FHt (0.3 < x < 0.7)	126-185
Polygorskite [Pal]	30-40
Sepiolite [Sep]	30-40
Illite [I]	10-40
Vermiculite	100-150
Laponite [Lap]	47-92
Micas (biotite, muscovite)	up to 5

Crucial for the swelling properties are the type of cations present in the interlayers. The amount of swelling is related to the type of interlayer cation: e.g. Na-rich Sm-clays expand more than those containing Ca. Both experiments and density functional theory calculations <sup>[13]</sup> investigating structural distortions and counterion positions of Mt with different alkali (Li<sup>+</sup>, Na<sup>+</sup>, K<sup>+</sup>) and alkaline-earth (Mg<sup>2+</sup>, Ca<sup>2+</sup>, Sr<sup>2+</sup>) cations suggest that the interlayer spacing increases quadratically with the counterionic radius, and that the counterion size influence distortions, rotations and thickness of both the tetrahedral and the octahedral sheets. It is also found that a counterion is not located symmetrically between layers, and that this is both related to the size and valency of the counterion.

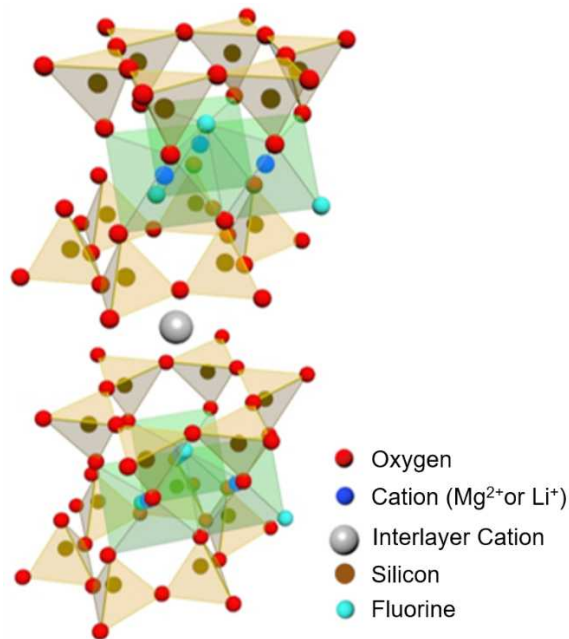


**Figure 2: Fluorohectorite (Fht) structure showing the position of the atoms described in Ref [12].**

Evidently these counterionic factors will influence the sorption of foreign molecules, such as H<sub>2</sub>O, in the interlayer <sup>[14]</sup>. For instance, an increase in basal spacing with the hydration energy of the saturating cation is observed <sup>[15]</sup>: Cs<sup>+</sup> < Rb<sup>+</sup> < K<sup>+</sup> < Na<sup>+</sup> < Li<sup>+</sup> < Ba<sup>2+</sup> < Sr<sup>2+</sup> < Ca<sup>2+</sup> < Mg<sup>2+</sup>, and there is a trend for increased swelling with an increase in cation hydration energy.

Fluorohectorite (Fht), represented in Figure 2, is a synthetic 2:1 layer Sm-clay that has been commercially available from Corning Inc.USA. In the present paper we will mainly discuss results based on Corning-Fht (Fht-C).

The group of Prof. Josef Breu at the University of Bayreuth in Germany has taken the synthesis of Fht a large step beyond the Fht-C, synthesizing Fht for which the magnitude of the well-defined sharp and homogeneous <sup>[16]</sup> layer charge allows for well-defined and well controllable crystalline as well as osmotic swelling depending on the layer magnitude of the charge <sup>[17]</sup>. The layer charge of the Breu-Bayreuth-Fht (Fht-B),  $[\text{Na}_x]^{inter}[\text{Mg}_{3-x}\text{Li}_x]^{oct}[\text{Si}_4]^{tet}\text{O}_{10}\text{F}_2$ , may typically be sharply designed in the range  $0.3 < x < 0.7$ , and the aspect ratio of Fht-B may be hundreds of micrometers <sup>[18]</sup>. This allows for several potential applications of Fht that are not available with other Sm, e.g. for applications in polymer nanocomposites, where the effect of nano-plate inclusions is mostly determined by their aspect ratio. This may for instance lead to significant improvements regarding reinforcement and gas-barrier properties as well as flame retardancy of polymer nanocomposites <sup>[19]</sup>.

Dzas et al. <sup>[20]</sup>, compared the influence of replacing OH groups in the silicate layers of Ht for F atoms. Ht and Fht samples with similar layer charge were prepared and hydrated to observe the effect of fluorination in the water adsorption. Fht adsorbed approximately 30% less water than its Ht counterpart and the water molecules directly hydrated the interlayer cations. The water molecules outside the hydration shell, behaved like water in a highly charged silicate layer. Figure 3 shows the effect of fluorination in the water uptake.

The fluorination of Ht can have many relevant applications, it is a way to fine tune the hydrophobicity of smectites. An evident application is barriers for water and the use of temperature resistance ceramics, since the dihydroxylation effect will not be present in this system.

There is a growing interest for synthetic clays, both from a purely scientific point of view, and from the point of view of applications <sup>[21]</sup>. This is driven by the possibility of designed homogeneity and controllable charge density of synthetic clays, as well as by the limited availability of some clays, such as smectites. There are several synthesis routes for various types of clays. Hts are perhaps the most studied and used synthetic clays. For instance, Laponite<sup>®</sup>, which is a registered trademark of a synthetic Ht (i.e. Laponite is not the name of a clay type), is presently produced industrially in large

amounts. Laponite® is commercially available and is manufactured from naturally occurring inorganic mineral sources. It is mostly used to improve the performance of a wide range of products such as a rheology modifier or a film forming agents. Laponite® layers typically have an aspect ratio of about 1:20, and a low layer charge making the layers easily exfoliated. Pure Laponite® aqueous suspensions can form transparent gels or sols depending on salt and clay concentration [22], making these systems good model systems for studies of soft matter anisotropic colloidal phenomena.

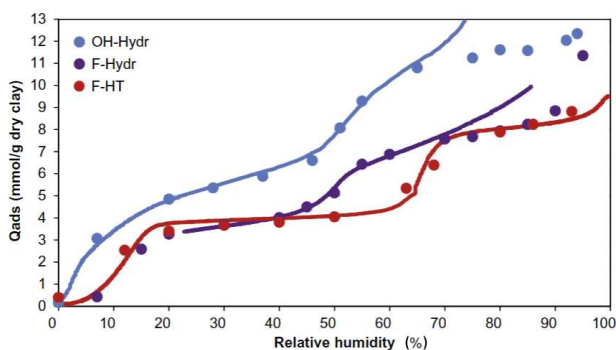


**Figure 3: Smectite water content [Qads] as function of relative humidity (RH). Effect of fluorination in the water uptake. Figure adapted from reference [20].**

FHt-C has been used to expand such studies [23, 24, 25, 26] into regions not available to Laponite®, limited by Laponite® layer’s aspect ratio, (typically 1:20), charge range (typically  $x$  near 0.2) and layer- platelet size (typically near monodisperse and centered at about 25 nm lateral diameter). FHt-B is synthesized from the melt [27], yielding the properties referred to above, i.e. large aspect ratio and large lateral dimensions as well as unique homogeneity and sharply controllable layer charge.

As is evident from the discussion above, clays are basically layered nanomaterials, (“nano in one direction”), that can exfoliate and form aqueous suspensions of nano-layers. Clays have a long scientific “track record” as an important geological material, obviously due to the large amounts present in geological formations.

The realization that clays are nano-materials and as such are very interesting

materials in materials science and technology, is a relatively new development in clay science. The clay layers can be functionalized at the nano-scale which determines the behavior of macroscopic clay systems, or the properties of nano-composites in which clay layers may be ingredients. This means that virtually every experimental characterization method that are used to understand nano-materials functionality and properties are used to study clays as well. In the following several such methods and results will be discussed: scattering techniques, thermodynamic characterization techniques, mechanical characterizations techniques, and molecular spectroscopy techniques, etc.

## II. Selected applications of Fluorohectorite clays

---

### II.1. Fluorohectorite for water retention

Hydration of clay minerals is one of the most studied topics in clays. For every application that clay minerals have, the interaction with water must be considered. Like other 2:1 silicates, FHT undergoes swelling when in contact with water. This swelling behavior has been demonstrated to be a function of the layer charge <sup>[16,17, 28, 29]</sup>, interlayer cation <sup>[18, 19, 30, 31, 32, 33]</sup> and sample preparation <sup>[30, 34, 35]</sup>. Several different techniques have been used to study the water-FHT system, such as x-ray diffraction (XRD) <sup>[18, 20, 30, 36, 37]</sup>, thermogravimetric analysis (TGA) and differential scanning calorimetry (DSC) <sup>[30, 38]</sup>, small angle x-rays and neutron Scattering (SAXS and SANS) <sup>[39, 40]</sup>, x-ray absorption <sup>[35]</sup>, incoherent inelastic neutron scattering (IINS) <sup>[41]</sup> and nuclear magnetic resonance (NMR) <sup>[31, 33]</sup>. Thus, the literature on this topic is rich and vast.

FHT has two swelling regimes: crystalline swelling and osmotic swelling. The former is observed with the variation of the basal spacing in vapor-hydrated samples, which is primarily connected to the number of water molecules in the interlayers. The latter is usually observed when clay mineral particles are dispersed in liquid water and their interlayer spacing increase to a point where they exfoliate. This depends on the layer and environmental temperature <sup>[25, 28, 29, 42]</sup>. In the crystalline swelling regime, where the interval of basal distances is lower than few nanometers, the intercalation is quantified by the basal spacing or d-spacing, which is the periodic distance of the silicate layers in the [00 $\ell$ ]

direction. For water molecules, particular molecular complexes and packings are energetically favored [43, 44], which results in particular discrete values of the d-spacing, that depends on the local relative humidity (RH) and temperature [32, 34, 42]. These discrete d-spacing values correspond to different hydration states of the clay particles, denoted as nWL (n = 0, 1, 2, 3, ...). The values of d-spacings, as well as dynamics of the transitions between hydration states, depend strongly on the nature of the cations that allow clay mineral particles to be held together. For Fht, several hydration studies have been performed with different types of intercalated cations [12, 18, 20, 30, 33, 34]. Many studies demonstrated that the hydration behavior is markedly different between cations such as Na<sup>+</sup>, Li<sup>+</sup> and Ni<sup>2+</sup>, as seen in Figure 4.

In Na-Fht, the hydration states are 0, 1 and 2 WL [12, 18, 20, 33]. Da Silva et al [18] used XRD data and proposed a configuration for the Na<sup>+</sup> cations in the interlayer. In the 1WL state of Na-Fht, the OH bond of the water molecules has been investigated using NMR-spectroscopy, and has been found to be almost perpendicular to the silicate layers [33], while the Na<sup>+</sup> cations are not located in the central space of the interlayer but coordinated with the oxygen atoms of the tetrahedral layers [12, 33]. In the 2WL state, the Na<sup>+</sup> cations move to the central region of the interlayer space, as shown Figure 5.

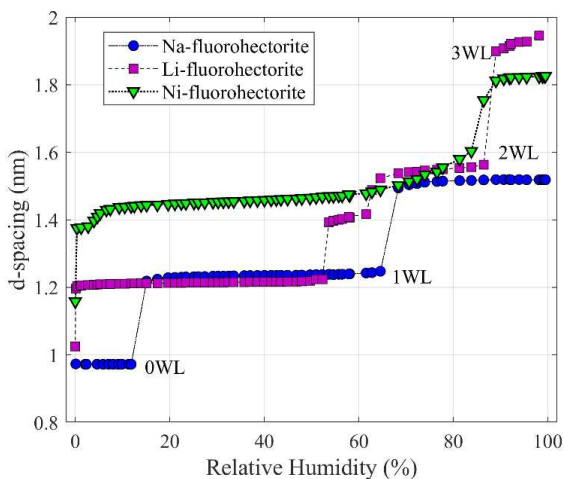


**Figure 4: Evolution of the d-spacing as function of relative humidity (RH) for Fht with different interlayer cations showing a step-wise expansion. Na-Fht and Li-Fht results are adapted from [34], while Ni-Fht results from [30].**

In Li-FHt, the hydration states are termed 0, 1, 1.5, 2 and 3 WL. The small ionic radius of  $\text{Li}^+$  cations gives interesting properties to this system. Tenorio et al. <sup>[31]</sup> suggested that even for small RH magnitude, the Li-water complexes exhibit a high degree of motion in the interlayers. The plateau between 1WL and 2WL seen in Figure 4 is attributed to an intermediate hydration state, called 1.5 WL. According to reference <sup>[31, 45]</sup>, the 1.5WL state in Li-FHt could be a stable hydrate state, where the  $\text{Li}^+$  goes from being part of an inner-sphere complex, which is a position close to the clay layers, to a position located near the middle of the interlayer space, thus forming an outer-sphere complex. However, other studies, such as Ref. [36], consider that the 1.5WL state is due to structural or chemical heterogeneities in the sample leading to interstratification of 1WL and 2WL and resulting in an average d-spacing.

The swelling kinetics of  $\text{Na}^+$ - and  $\text{Li}^+$ - FHt was measured by Michels et al. <sup>[34]</sup>, using the lowest value of RH that causes the transition from the dehydrated 0WL to 1WL. It was observed that it takes  $\approx 7$  hours for Na-FHt to complete the transition, while for Li-FHt it is much faster (less than 1 hour). This has a strong influence on the diffusion of water through small tubes filled with initially dry powder samples. Water vapor diffusing through an Na-FHt powder filled tube behaves as predicted by Fick's law, hence normal diffusion, while water vapor diffusing a Li-FHt powder filled tube behaves anomalously, which had to be modelled using an anomalous sub-diffusion approach <sup>[46]</sup>.

FHt with  $\text{Ni}^{2+}$  cations have also been studied <sup>[30, 35, 47]</sup>. Combining EXAFS and XRD <sup>[35]</sup> it was found that  $\text{Ni}^{2+}$  forms a brucite-like structure in the form of  $\text{Ni}[\text{OH}]_2$ . This structure coexists with the clay mineral particles and is formed during the cation exchange process from Li-FHt to Ni-FHt. In a systematic study of hydration of Ni-FHt, Altoé et al. <sup>[30]</sup> found that this system behaves significantly different from previous studies of Na-FHt and Li-FHt smectites. As seen in Figure 4, for Ni-FHt the stepwise expansion is not observed, rather a continuous transition between hydration states is measured. These findings suggest the existence of various forms of  $\text{Ni}^{2+}$ -water complexes. The presence of similar liquid-type complex structure has been previously reported based on a neutron diffraction study of the interlayer structure of highly hydrated Ni-Mt.<sup>48</sup>

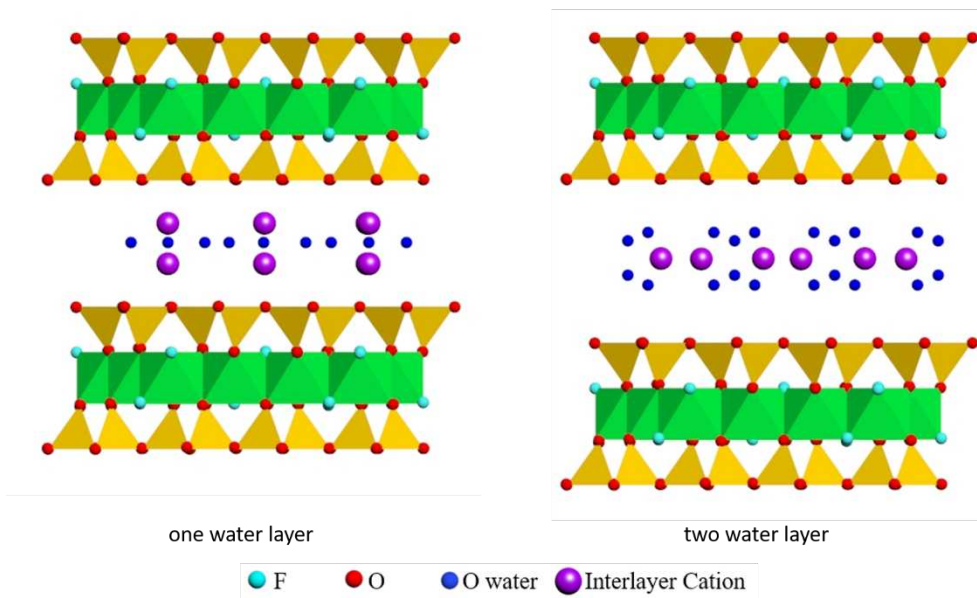


**Figure 5: Structure of water in the (a) one water layer (1WL) and (b) two water layers (2WL) in Na-FHT.**

## II.2. Fluorohectorite for drug delivery

Developing new Active Pharmaceutical Ingredients [API] is an expensive and time-consuming process. Considering all steps involved in the discovery, i.e. development and regulatory approval of a new drug formulation, it is estimated that might take a decade and cost over \$ 1.4 billion to launch a new API in the market <sup>[49]</sup>. On the other hand, increasing the efficiency of an API already in use is cheaper and faster, creating an alternative to developing new formulations. In this regard, selecting appropriate drug carriers is fundamental, as long as it promotes controlled release, protects the API from chemical degradation, guarantees its release in the correct action site, consequently promoting the drug efficiency <sup>[50, 51]</sup>. In this scenario, considering its structure and physicochemical properties, FHT can be seen as a promising material for such applications.

In general, the use of clay minerals in pharmaceutical formulations is related to their high specific area and absorbing capacity, chemical inertness, low

toxicity, even when orally administrated, and low price, when considering the naturally occurring clay minerals <sup>[51, 52, 53]</sup>. Moreover, regarding the possibility of precisely controlling their physicochemical properties, such as layer charge, porosity, particle size, impurities, etc., synthetic clays are possibly more suited for health applications. Nevertheless, given the difficulty and cost involved in synthesizing these minerals, the natural clays are still dominating this area, a situation that might change through scaling up of synthetic clay mineral applications.

Taking into account that the oral route is the most important way of drug administration, FHt shows an advantage in comparison with other clay minerals, which is possibly higher resistance to acidic attack in low pH environments, such for gastric juice. It has been reported that at low pH environments, free H<sup>+</sup> in the solution might migrate to the clay mineral structure, thus dissolving the clay particles <sup>[54, 55]</sup>. FHt, however, may be more resistant to acid dissolution than other smectites due to the presence of fluoride ligands instead of hydroxyl ones, such as in Mt and natural Ht <sup>[56]</sup>.

Although FHt presents important properties for its use in drug delivery applications, only a few studies are reported in this field <sup>[56, 57]</sup>. The first studies on capture and release of APIs by FHt were performed using mostly ciprofloxacin (CIPRO), a broad-spectrum antibiotic agent, as a model drug. Recently such investigations have been extended to other drug molecules, such as sulfamethoxazole and trimethoprim. These studies have shown encouraging results, evidencing the potential and applicability of FHt as an API carrier.

It has been demonstrated that the capture of CIPRO by FHt is more efficient at acidic than neutral environments, with FHt capturing up to 0.49 g of CIPRO per gram of FHt, and highly inefficient capture at alkaline conditions <sup>[52, 56, 57, 58, 59, 60]</sup>. There is substantial evidence pointing out that the capture of APIs at low pH occurs mainly via cation exchange, with the drug molecules replacing the interlamellar cation and acting in its place to maintain the charge balance of the FHt particles <sup>[52, 56, 58]</sup>. Despite CIPRO's capture ability at neutral environments, the higher efficacy in acidic conditions indicates that the ionic nature of the API is an important parameter to be considered when preparing the clay-drug composites <sup>[56]</sup>. Furthermore, release studies demonstrated that the drug release is slow, pH-dependent, controlled and thermally activated <sup>[52, 58]</sup>

Regarding toxicity of FHT and FHT-drug composites, *in vivo* and *in vitro* studies demonstrated that FHT is not harmful, even when it has  $\text{Li}^+$  as interlamellar cation [58, 59]. Additionally, the effectiveness of FHT-CIPRO against important human pathogens, such as *E. coli* and *P. aeruginosa*, remained the same as the effectiveness of CIPRO alone. This indicates that the clay-drug interaction in all steps of the capture and release process does not affect the API molecules, thus demonstrating the applicability of FHT as a carrier capable to protect and properly delivery CIPRO molecules. In the future it is expected that this research will be successfully extended to other APIs. In fact, studies with tramadol, sulfamethoxazole and trimethoprim have pointed to similar conclusions to the ones obtained for CIPRO [57,60]. Certainly, further studies are needed in order to evaluate the extent of FHT capabilities as a drug carrier and its application in the pharmaceutical industry.

### II.3. Clay for carbon capture and retention

Earth's ecosystems are facing severe challenges as a non-sustainable consumption and overpopulation has pushed to the brink of failure. Human activity is changing the environment through an ever-increasing list of destructive activities, such as deforestation, greenhouse gas emission, invasion in natural habitats and pollution [61, 62, 63, 64]. In this context,  $\text{CO}_2$  sequestration using specific mesoporous materials is one of the measures now being considered in order to partially alleviate this situation. Among the mesoporous materials suitable for carbon dioxide ( $\text{CO}_2$ ) capture and retention, we find porous structures like MOFs, COFs [65], Zeolites, activated carbon, amyloid fibers [66], amine-based nanofibrillated cellulose [67] and nanoparticles like co-IonomIM-17% ( $\text{Mg}^{2+}$ ) [68], spheres [69] and copper silicates [70]. The common feature of all these structures is the presence of suitable pore diameters that facilitate the physisorption of  $\text{CO}_2$ . Clay minerals can provide further technological aid to remediate some of these effects, as the swelling properties of smectites allow the basal interlayer spacing to increase upon  $\text{CO}_2$  uptake [71, 72]. For instance, Monte Carlo simulations predict a higher  $\text{CO}_2$  uptake for expanded interlayer spacing of Mt [73]. Besides, clay minerals are also present in cap-rock formations suitable for carbon sequestration [74].

Gas adsorption happens under certain conditions of pressure and temperature, and low-density materials can adsorb an amount of gas that can

be even higher than the weight of the material itself. It means that the *weight ratio* gas (g)/ host material (g) is a number higher than 1. In the literature this quantity is also represented by the *weight fraction*: gas(g)/(gas(g)+material(g)). A high weight ratio means that the material has a high gravimetric capacity, which can be displayed as the number of mole of gas molecules per gram of material (mmol/g). Here we call this quantity the *molar uptake*. Thus, MOFs exhibit the highest gravimetric uptake since they are materials with very low density. MOF-210<sup>[75, 76]</sup> is able to adsorb 65 mmol of CO<sub>2</sub>/g of host material, a little more than the activated carbon<sup>[77]</sup> with 55 mmol of CO<sub>2</sub>/g of host material. Far behind in this category of gravimetric uptake, are the clays and other materials like the commercial Zeolite 13X<sup>[78]</sup> with 7 mmol of CO<sub>2</sub>/g. According to the application, it is also useful to display the *volumetric capacity* of the material, which is the weight ratio multiplied by the density of the material. High volumetric capacity is advantageous for applications where large volumes can be an issue. To date, the material with the highest volumetric CO<sub>2</sub> capacity is claimed to be the activated carbon<sup>[77]</sup>. However, clays also exhibit high volumetric capacity for CO<sub>2</sub>, as observed for Ni-FHt<sup>[68]</sup>.

Revising the main recent publications, cf. Table 2, it is observed that the CO<sub>2</sub> uptake by clays ranges from 0.2 mmol/g to 6.4 mmol/g. As illite (I) is harder to swell, its uptake is lower and varies from 0.2 mmol/g<sup>[79]</sup> to 0.4 mmol/g<sup>[80]</sup>, while Kaol<sup>[81]</sup> and Bent<sup>[82]</sup> have similar uptake. Mt is the most studied clay species and present the maximum CO<sub>2</sub> uptake of 2 mmol/g<sup>[83]</sup> for the pure material<sup>[84, 85, 86, 87]</sup>, and higher values for functionalized structures<sup>[80, 88]</sup>, like 3.2 mmol/g for the polymer modified PEI-Mt<sup>[89]</sup> or 3.8 mmol/g for the nano-Mt<sup>[90]</sup>. An enhanced uptake can also be observed by exchanging the interlayer cations in Ht clay<sup>[69]</sup>.

Pillared tetraethylammonium Ht<sup>[91]</sup> shows an uptake of 4 mmol/g. Another important material property for carbon sequestration is the ability of adsorbing flue gas, at ambient conditions. This was reported for some clays, where an increased uptake occurs as the pressure of CO<sub>2</sub> increases. For example, sepiolite<sup>[79]</sup> has an uptake of 3 mmol/g at 65 bar, while Ni-FHt shows an uptake up to 6.4 mmol/g at a pressure of 50 bar of CO<sub>2</sub>. This enhanced uptake is also observed by adjusting other conditions, like temperature, or by modifying the material charge density, surface area, porosity and binding sites. Bentonite porous clay heterostructures (PCH) show an uptake of 1.6 mmol/g after functionalization<sup>[92]</sup> due to the strong interactions between amine species and CO<sub>2</sub> molecules. FHt clearly shows a larger adsorption for CO<sub>2</sub> than other

**Table 2: Example of high capacity CO<sub>2</sub> retention materials**

<b>Materials</b>	Molar Uptake [mmol/g]	Gravimetric capacity [weight ratio]	Density [g/cm <sup>3</sup> ]	Vol. capacity [ton/m <sup>3</sup> ]	P [bar]
<b>CLAYS</b>					
Ni-FHt (Cavalcanti, 2018) <sup>71</sup>	6.4	0.28	2.8	0.79	55
MOF-aminoclay CuBTC@AC-2 (Chakraborty, 2016) <sup>73</sup>	5.4	0.24	-	-	1
Na-FHt (Cavalcanti, 2018) <sup>71</sup>	4.8	0.21	2.8	0.58	53
Pillared tetraethylammonium Ht (Sozzani 2006) <sup>91</sup>	4.1	0.18	-	-	0.8
Polymer modified Mt (Wang, 2014) <sup>89</sup>	3.2	0.14	-	-	1
Mt (Stevens, 2013) <sup>83</sup>	2.4	0.11	2.8	0.30	1
Illite (Busch, 2008) <sup>80</sup>	0.4	0.02	2.2	0.04	90
<b>OTHER MATERIALS</b>					
MOF-210 (Furukawa, 2010) <sup>75</sup>	65	2.87	0.25	0.72	50
Mesoporous carbon (Cox, 2017) <sup>77</sup>	55	2.42	0.38	0.93	50
Zeolite 13X (Cavenati, 2004) <sup>78</sup>	7.0	0.31	2.0	0.61	40
Covalent organic frameworks, COFs (Zeng, 2016) <sup>65</sup>	2.1	0.09	-	-	1

clay minerals. In a recent simulation paper <sup>[93]</sup>, by investigating the effect of the substitution of F<sup>-</sup> and OH<sup>-</sup> in Ht and thereby tuning the hydrophobicity, it was shown that by increasing the F<sup>-</sup>/(F<sup>-</sup> + OH<sup>-</sup>) ratio in the octahedral layer, the CO<sub>2</sub>/(CO<sub>2</sub> + H<sub>2</sub>O) ratio adsorbed in the interlayer increases, while the total amount of adsorbed molecules decrease.

The cation also plays an important role, for instance Ni-FHt adsorbs more CO<sub>2</sub> than Li-FHt or Na-FHt. It was also observed <sup>[94, 95, 96]</sup> that larger cations such as Cs<sup>+</sup> adsorb CO<sub>2</sub>, whereas smaller molecules such as Na do not without the presence of water. This is contrary to what is observed for FHt <sup>[71, 72]</sup>, where the clay with the smaller Li<sup>+</sup> and Ni<sup>2+</sup> cations can adsorb a larger amount CO<sub>2</sub> when compared to the values reported for the larger Na<sup>+</sup>. This suggests that the clay structure, the isomorphic substitutions, the clay's CEC value, purity and the interlayer environment play a combined role for the adsorption of CO<sub>2</sub>. The relation between solvation energy of the cation and CO<sub>2</sub> is however not completely understood.

### III. Characterization Methods

---

#### III.1. X-rays/neutron scattering for structure/slow dynamics

One of the most common techniques to study the swelling of FHt clays, due to interactions with small molecules, is x-ray or neutron diffraction (XRD or ND), since the layered clay periodicity is of the order of 1nm. From a diffraction measurement, where the peaks are located at the Bragg condition  $2d \sin(\theta) = m\lambda$ , the intensities of the scattered beam are usually plotted as function of  $2\theta$  or  $q$ . The former is the angle between the incident beam and the scattered beam, while the latter is the scattering vector, which has a scalar value given by  $|q| = \frac{4\pi \sin(\theta)}{\lambda}$ . Normally, the intensity of a diffracted x-ray beam can be described as:

$$I(q) \propto |G(q)|^2 L_p(q) \Phi(q) \quad (1)$$

$$G(q) = 2 \sum_{j=1}^n n_j f_j \exp \left[ -W_j \left( \frac{q}{4\pi} \right)^2 \right] \cos(qZ_j) \quad (2)$$

where  $f_j$  is the atomic scattering factor and refers to the number of atoms of the type  $j$  located at a distance from the center of symmetry along the  $(00\ell)$  axis.  $W_j$  is the Debye-Waller temperature correction factors. The summation is over all atoms of the unit cell <sup>[97]</sup>. Since the unit cell includes the interlayer space, the structure factor also determines the relative strengths of the  $(00\ell)$  peaks between different hydration states. This makes the  $(001)$  peaks of a dry clay mineral weaker compared to the hydrated <sup>[18, 30]</sup>. If the details of the unit cell are known, and the recorded Bragg intensities extends to high angles (several  $(00\ell)$  peaks), the structure factor can be used to locate the amount and position of interlayer molecules in the clay mineral <sup>[18, 36, 98]</sup>.

The Lorentz polarization factor can be expressed as:

$$L_p(q) = \frac{P}{\left( \frac{\lambda q}{4\pi} \right)^{\nu+1} \sqrt{1 - \left( \frac{\lambda q}{4\pi} \right)^2}} \quad (3)$$

where  $P$  is the polarization contribution that depends on the x-ray source. The exponent  $\nu$  is related to the number of crystals favorably oriented for the diffracted intensity to be accepted into the detector at a given Bragg angle. It varies from  $\nu = 1$ , for a perfect powder, to  $\nu = 0$ , for a perfect crystal <sup>[99]</sup>. For natural clays the correct number is between these two cases <sup>[97]</sup>.

The interference function  $\Phi(q)$ , is responsible for the formation of Bragg peaks. Typically, it is fitted with a pseudo-Voigt function, which is a linear combination of a Gaussian and a Lorentzian function <sup>[18]</sup>:

$$\Phi(q) = \mu \frac{2}{\pi} \frac{\Gamma}{4(q - q_c)^2 + \Gamma^2} + (1 - \mu) \frac{\sqrt{4 \ln 2}}{\sqrt{\pi} \Gamma} \exp\left[\frac{-4 \ln 2 (q - q_c)^2}{\Gamma^2}\right] \quad (4)$$

where  $q_c$  is the peak position and is related to the d-spacing by  $q_c = 2\pi/d$ -spacing. The parameter  $\mu$  is the proportion of Lorentzian and Gaussian curves. For  $\mu = 1$  the curve is full Lorentzian, while for  $\mu = 0$  the curve is full Gaussian.  $\Gamma$  is the convoluted full width at half maximum <sup>[100]</sup>:

$$\mu = 1.36603 \left(\frac{\omega_L}{\Gamma}\right) - 0.47719 \left(\frac{\omega_L}{\Gamma}\right)^2 + 0.11116 \left(\frac{\omega_L}{\Gamma}\right)^3 \quad (5)$$

$$\Gamma = \left(\omega_G^5 + 2.69269\omega_G^4\omega_L + 2.42843\omega_G^3\omega_L^2 + 4.47163\omega_G^2\omega_L^3 + 0.07842\omega_G\omega_L^4 + \omega_L^5\right)^{\frac{1}{5}}$$

The Voigt function can also be used to obtain the deconvoluted Gaussian and Lorentzian widths <sup>[101]</sup>. Other forms of the pseudo-Voigt function, where  $\Gamma$  is simply replaced by  $\omega_L$  in the Lorentzian part and by  $\omega_G$  in the Gaussian part, makes the  $\Gamma$  expansion above unnecessary. The  $\omega_L$  and  $\omega_G$  parameters denote sample and instrumental contribution to the line broadening respectively. The Lorentzian components  $\omega_L$  can be considered to mainly depend on the size or thickness of crystallized domains, which is related to their lattice strain or disorder in the lattice spacing. The relation between the size and lattice strain may be determined by plotting the experimental data in the form of a Williamson-Hall plot <sup>[102]</sup>, and fitting the experimental data to the following relation in terms of the scattering vector  $q$ .

$$\omega_L = \frac{2\pi}{Nd} + \xi q \quad (6)$$

The slope of the line  $\omega_L$  versus  $q$  thus gives the lattice strain  $\xi$ , which is defined as  $\xi = \Delta q/q_c$ , and the intercept at  $Nd$  estimates the mean particle thickness. This approach has been used to study the average particle

thickness and the lattice strain of Fht as function of water content <sup>[18, 30]</sup>.

Combined with the internal periodicity of the layered clay particles determined by diffraction techniques (atomic resolution), the shape and colloidal particle sizes (lower resolution), as well as particle interaction, can be studied by small angle scattering (SAS) techniques. Such studies can be performed employing neutrons or x-rays. These are complementary probes, where the main difference is the contrast obtained between the clay particles and the surrounding matrix. The scattering from neutrons is from the nucleus, rather than from the electron cloud in an atom, which means that there is no correlation between the neutron scattering cross-section and the atomic number of the scatterer. In contrast with x-rays this makes the study of lighter elements possible. Furthermore, as the neutron scattering cross section is different for different isotopes, these isotopic contributions can be distinguished experimentally. These unique properties make neutrons ideal for probing the structure and dynamics in hydrogenous solids and liquids and make this technique extremely useful for analyzing the dynamics of liquids in confinement <sup>[103]</sup>. The scattered intensity from the clay particles can generally be regarded as consisting of a contribution from the particle shape and size (form factor  $P(q)$ ), combined with a contribution from the particle interactions (structure factor  $S(q)$ ), and a pre-factor containing the scattering contrast. The latter is given by the square of the difference in the so-called scattering length density  $\rho$ , which for x-rays depends on the electron density and for neutrons on the scattering length of the isotopes in question, as mentioned above.

$$I(q) \propto |\Delta\rho|^2 P(q)S(q) \quad (7)$$

Note that the structure factor  $S(q)$  used in SAS techniques has a slightly different meaning than the factor  $G(q)$  employed in diffraction methods (cf. eq. 1). For oriented particle systems, one should take into account that the structure factor depends on the spatial direction, and it may then be convenient to operate with two structure factors, typically parallel and orthogonal to the orienting field <sup>[104]</sup>. Also, clay minerals can be very polydisperse and this would screen many features of the scattering pattern, such as  $S(q)$  and  $P(q)$ . Therefore, it is convenient to work in dilute systems, where  $S(q) \approx 1$ , and  $P(q)$  can be modelled considering the polydispersity effect.

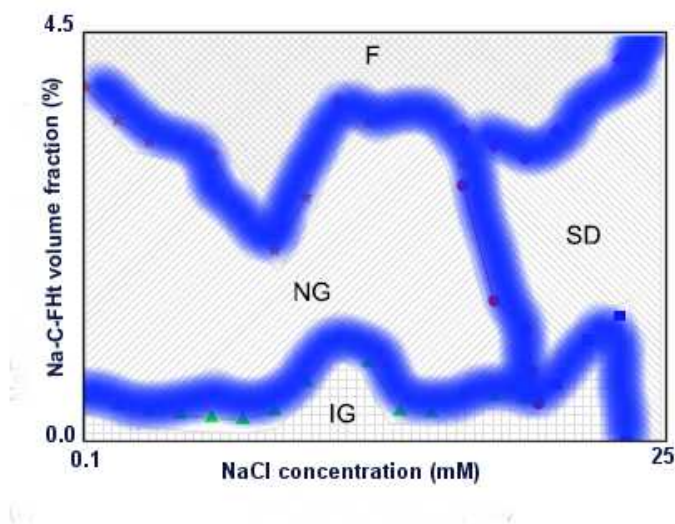


**Figure 6: Phase diagram of FHT-C, measured by combined SAXS and x-ray absorption, adopted from Reference 26. F = Flocculated particles, NG = Large domain repulsive Nematic Gel, IG = Isotropic Gel, SD = Small Domain attractive Nematic.**

FHT-C has a relatively high layer charge <sup>[105]</sup> preventing exfoliation, thus in saline aqueous suspensions of FHT-C there is no exfoliation and the particles remain intact in stacks consisting in average of about 100 platelets <sup>[106]</sup>, unless the temperature is increased <sup>[25]</sup>. The aspect ratio of the stacks is polydisperse in the ranging from about 1:10 to about 1:100, and these particles may form isotropic or nematic phases depending on clay concentration (induced by gravitational sedimentation), or salinity <sup>[23, 24, 26]</sup>, see Figure 6. It has also been found that magnetic field scan orients the FHT-C particles in aqueous suspensions, e.g. inducing Fredricks transitions <sup>[107]</sup>.

### III.2. Infrared and Raman Spectroscopy

Both Infrared (IR) and Raman spectroscopy (RS) are techniques that probe vibrational modes of a material or molecules. However, while IR results from the absorption/transmission of the infrared radiation by molecular bonding, RS is based on the inelastic scattering of monochromatic radiation <sup>[108, 109, 110]</sup>. When applied to the study of clay minerals, and differently from XRD, SEM and TEM <sup>[111]</sup>, both techniques offer the benefit that no specific sample preparation is required. Additionally, these are among the cheapest techniques that provide information on the molecular level. These advantages make these techniques

very attractive <sup>[110]</sup>.

The IR spectrum of materials, including clay minerals, is sensitive to its chemical composition and structural arrangement <sup>[112]</sup>. An IR spectrum might be understood as a fingerprint of the material under study, making IR a widely used technique for materials identification and characterization. Regarding clay minerals, via IR spectroscopy it is possible to identify the vibrational modes of the OH groups, the silicate anion, the octahedral and interlayer cations, as well as the interlamellar water. The OH vibrations of clay minerals are clearly observed in the near-infrared (NIR) region from 11000 to 4000  $\text{cm}^{-1}$ , while the middle-infrared (MIR) region from 4000 to 300  $\text{cm}^{-1}$  holds information on their fundamental vibrational modes <sup>[54, 112, 113, 114, 115]</sup>.

Since Fht is derived from Ht, thus presenting similar structure and composition <sup>[12, 54, 113]</sup>, their IR spectra present many similarities. The larger differences being that Fht has fluorine instead of hydrogen in its structure, thus the IR spectra of Fht does not show the vibrational modes of H, but instead the vibrational modes of structural fluorine groups. Therefore, in Fht any OH-related mode is either to cationic or to surface water. As an example, Figure 6 illustrates the main features of the IR spectra for Fht in the MIR region <sup>[30, 52, 54, 60, 113, 115, 116]</sup>. This information is useful for instance to identify the purity degree of the Fht structure, study water populations within its layers, or to get information concerning guest molecules either on the clay surface or within its layers <sup>[12, 30, 52, 54, 60, 112, 113, 115, 116]</sup>.

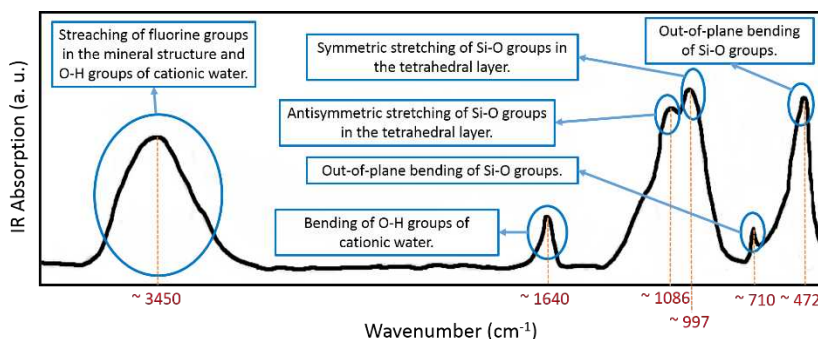


**Figure 7: Representation of the Fht IR spectra in the MIR built based on the references [30, 52, 54, 60, 113, 115].**

In turn, RS gives complementary information to IR; however, it has been a less popular technique among clay scientists. The RS signal is weak, the samples suffer photo-degradation and quite often an overlapping fluorescence masks the Raman signal <sup>[117]</sup>. In recent decades Fourier transform Raman spectrometers and Raman microscopes have been able to overcome these difficulties and the instrumentation has become more available. These technological advances have resulted in a growing number of studies. For instance, Mt, nontronite, natural and synthetic saponite have been studied by RS and the observed bands have been assigned <sup>[118, 119, 120, 121, 122]</sup>. There is only one reported RS study of Ht <sup>[123]</sup>, where identification of di- and tri-octahedral phyllosilicates was possible. As a result of the low RS signal from the clay mineral, an advantage of this technique is that it can be used to probe other species in the system with little spectral interference from the clay mineral itself. This is how RS has been employed to study FHt <sup>[124]</sup>, where the interaction between organic molecules in the interlayer and the clay has been determined. As RS is becoming a more common technique among clay scientists, it can be expected that the results will help understanding the interactions in the elusive interlayer region.

### III.3. Neutron Spectroscopy, NMR and Molecular Dynamics

Swelling of clay layers and water diffusion, either in bulk or confined, occur on time scales of ps to ms, and computational modeling and spectroscopic methods such as NMR spectroscopy <sup>[31, 33, 125]</sup> and INS <sup>[126, 127, 128]</sup> have proven to be especially effective. Computational tools such as classical molecular dynamics (MD) simulations complement experimental approaches by providing molecular-scale insight currently inaccessible by existing spectroscopic methods. For instance, as shown for FHt <sup>[129]</sup>, the combination of MD with neutron spectroscopy allows accurate analysis of the mixed dynamics (rotation and librations as well as distinction of water in different environments), and consequently to model accurately more and more complex systems approaching the real natural clays <sup>[129]</sup>. While for Na-Ht <sup>[130]</sup>, it was shown that computational results together with experimental results obtained with NMR spectroscopy support a model for interlayer H<sub>2</sub>O structure and indicate that H<sub>2</sub>O molecules undergo simultaneous fast librational motions and site hopping. Additionally, density functional calculations (DFT) and classical

MD have been successfully applied to study the structure and dynamics of water interacting with kaolinite surfaces and confined in the interlayer of Hal [131]. Finally, we mention that by combining Monte Carlo and MD simulations it was shown that CO<sub>2</sub> considerably influences the diffusion of water in Na-Mt [132].

The neutron scattering response can be inelastic or elastic depending on the finite energy transfer between the neutrons and the sample, as shown in Figure 8. By analyzing the inelastic signal, information on the periodic motions of the molecules in the sample with a finite energy transfer can be obtained. Similar to other spectroscopic techniques, the results from inelastic neutron scattering (INS) measurements are basically a spectrum formed by several peaks, which broaden with increasing temperature due to the Debye-Waller factor. INS, however, offers a unique advantage that cannot be achieved by other widely used optic spectroscopies techniques, namely: INS has no selection rules due the nature of the interaction between the probe and the sample (neutron-nucleus interaction). Thus, in principle all transitions are observable. Additionally, due to the large H-cross section, INS is extremely useful for looking hydrogen motions [133]. Finally, the INS amplitude is proportional to the motion and the scattering cross section of the atoms involved. These properties make INS an extraordinary test for the quality of *ab initio* calculation of vibrations in molecules [134], which have been applied to characterize different cation exchanged Mt-samples confirming that both confinement and cation type modify the librational behavior of water [135].

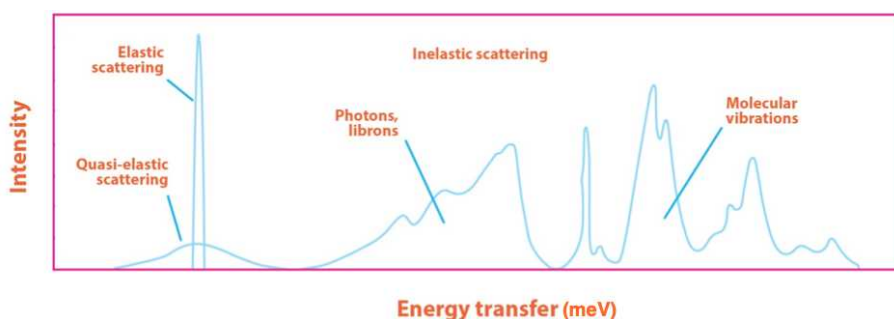


**Figure 8: Schematic of the neutron scattering spectrum from samples dominated by hydrogen atoms. As explained in the text the spectrum can be separated in elastic, quasi-elastic and inelastic responses.**

The elastic component is related to the thermal fluctuations of the atoms around their equilibrium position. If the scattering from the analyzed sample is mostly incoherent, as in the case of clay minerals, the evolution of the measured signal as a function of energy, time and/or temperature allows probing the mobility of the hydrogen atoms. This is the so-called elastic fixed window (EFW) approach that provides an overview of the molecular mobility in the sample as a function of temperature and consequently to determine the onset of the proton mobility by noting points of inflexions in the elastic scattering response, i.e. temperature values where deviation from the classical Debye -Waller behavior occurs. For instance in the case of Mt and Hal, using this methodology it was clearly demonstrated that the cations  $\text{Na}^+$  in this particular study) in the interlayer regions act as gate keepers and to a certain extent control the water mobility <sup>[126]</sup>, while in the study of intercalation of the capture of CIPRO by Fht <sup>[56]</sup> insight on how the water dynamics is affected by the presence of the drug molecules located in Fht was obtained. Additionally, very recently, the hydration states of swelling Mt clay minerals were obtained using the EFW method <sup>[127]</sup>. By evaluating the elastic intensity as a function of time, the authors followed the adsorption, movement and release of water in Na-Mt and in this way obtained important information on the design of for instance hydraulic barrier technologies <sup>[128]</sup>.

In the particular case of broadening of the elastic scattering line, random diffusive motions of the molecules on a time scale of nanoseconds to picoseconds are probed. This technique, called quasi-elastic neutron scattering (QENS), is well suited to gather quantitative information about the correlation times and length scales of the diffuse motion occurring in hydrogenous materials in confined geometries, such as water confined within the layers of different clay minerals, e.g. Mt, <sup>[126]</sup> as well as water confined in clay mineral/polymer nano-composites <sup>[128]</sup>. The analysis of the quasi-elastic (QE) response allows distinguishing free, confined or chemically bound hydrogen dynamics within the observation time of the selected spectrometer. Analysis of the QENS signal also allows for obtaining qualitative information relating to the geometrical mechanism of the motion.

NMR spectroscopy, on the other hand, complements the XRD and ND data at a molecular level, probing the structure, conformation and dynamics of the intercalated surfactant ions. NMR studies in natural clay minerals are vulnerable to paramagnetic  $\text{Fe}^{3+}$  normally present in common Mt. This problem can however be circumvented by studies using the related, non-paramagnetic

Ht clays. An intrinsic advantage of  $^1\text{H}$  and  $^7\text{Li}$  NMR is their ability to probe cation mobility as well as water mobility averaged over a time scale which is long compared to what is normally accessible by molecular simulations, complementing the QENS results. Furthermore, an interesting aspect of Fht is that the OH groups of hectorite have been replaced by fluorine, making the interpretation of proton spectra less ambiguous. For instance, hydroxylated Ht exhibits two  $^1\text{H}$  NMR signals, whereas synthetic saponites are characterized by a single peak in the same region <sup>[136]</sup>. Another powerful way to study fluorinated 2:1 layered materials is the use of  $^{19}\text{F}$  MAS-NMR that enables the determination of the coordination of structural fluorine by exploring the signal related to the octahedral sheet compositions and how the octahedral elements (Al, Mg, Fe, Li...) are bonded to the fluorine <sup>[137]</sup>. For instance, a combination of chemical analysis with results from a  $^{19}\text{F}$  spectrum were successfully used to determine unknown octahedral composition Li-Fht <sup>[138]</sup>. Further results of great interest are from a comparative study obtained using  $^1\text{H}$  and  $^2\text{H}$  NMR measurements in Na-Fht and Na-vermiculite (one of the most studied clay minerals using NMR). While a proton exchange mechanism can be used to describe the central line in the proton spectra of 2WL in both samples, <sup>[139]</sup> the fraction of protons participating in the exchange process as well as the fraction of water molecules outside the hydration sphere, i.e. the presence of interlamellar water, are noticeably greater in Na-Fht <sup>[33]</sup>. Furthermore, the smaller relative weight of the central peak observed in  $^1\text{H}$  NMR spectra of Li-Fht compared to Na-Fht can be considered a possible mechanism of the lower electrical conductivity in Li-Fht at low RH <sup>[31]</sup>.

## IV. Conclusion

Fluorohectorite (Fht) is a synthetic smectite clay commercially available (Fht-C with relatively high and somewhat inhomogeneous layer charge,  $x \approx 0.6$ ). Large steps forward in the synthesis control and design of sharp charge homogeneity and layer aspect ratio have been made (Fht-B with sharp and tunable layer charge  $0.3 < x < 0.7$ ). These factors manifest themselves in the onsets and behaviors of crystalline swelling as well as for osmotic swelling (i.e. layer exfoliation).

Here we have mainly discussed results obtained on FHT-C. In particular, we have pointed to works that investigate the influence of interlayer cation type for molecular capture and retention ( $\text{H}_2\text{O}$ , bioactive molecules,  $\text{CO}_2$ ). The type of intercalated cation is a deciding factor for the crystalline swelling due to water vapor /gas pressure exposure. We have shown that spectroscopic characterization (IR, Raman, inelastic and quasi-elastic neutron scattering, NMR) coupled with molecular dynamics simulations give complementary information to scattering experiments (XRD or neutron scattering) regarding molecular interactions with clays, either coupled to residing charge compensating cations ( $\text{H}_2\text{O}$  and  $\text{CO}_2$ ), or through cation exchange processes (bioactive molecules). We suggest that FHT could be a better choice than natural clays for pharmaceutical purposes as a result of their controllable layers charge. We also point to recent work demonstrating that FHT has extremely high volumetric capture capability for  $\text{CO}_2$  compared to alternative synthetic or natural materials, and we suggest that this potentially can be used for greenhouse gas separation and  $\text{CO}_2$  capture, retention, transport.

We have also discussed saline aqueous suspensions of FHT-C. FHT-C unlike low charge FHT-B does not exfoliate even in pure  $\text{H}_2\text{O}$ , thus FHT particles remain intact comprised of about 100 layers, thus resembling suspensions of some natural clays such as illite (I). FHT suspensions form isotropic or nematic phases depending both on the clay and on the salt concentration.

Particularly it is the purity, and layer charge control, including the possibility of extreme homogeneity (FHT-B) that makes FHT interesting for materials technology applications such as flame-retardant composites, gas barrier polymer clay nanocomposites, and others. Smectite clays such as bentonite (i.e. montmorillonite, Mt) are commonly used as barriers for chemical wastes, and are now also considered as secondary barriers for long-term safe nuclear waste storage (NWS) <sup>[8]</sup>. Here we point out that for NSW application, there might potentially be an important role to play for FHT. The amounts of clays needed are not enormous, and there is indeed need for geological time scale control and design of the clay used for this purpose, both in terms of nanoscale functionalization

(for molecular capture) and in terms of suspension behavior and sedimentation, and the self-healing properties of clay powders in suspension.

All-in-all the very active ongoing scientific work on natural <sup>[140, 141]</sup> and/or synthetic <sup>[142, 143]</sup>, including FHT <sup>[144, 145, 146, 147]</sup>, and in particular on FHT-B, should extend dramatically the mentioned applications and hint to new ones. FHT is an important material in clay science that definitely underlines the statement that “*clays may be considered the material of the 21<sup>st</sup> century*” <sup>[8]</sup>.

**Cite this paper:** P. H. Michels-Brito , L. Michels , K. W. B. Hunvik, E.C. dos Santos, B. Pacáková, L. P. Cavalcanti, K. D. Knudsen, H. N. Bordallo and J. O. Fossum, OAJ Materials and Devices, Vol. 5(2) (2021) - chap No21, p 601 in “*Perovskites and other framework structure crystalline materials: new trends and perspectives*”- DOI:10.23647/ca.md20201501

### Acknowledgements:

P.H.M.B PhD studies is supported by NTNU. Financial support from the Norwegian Research Council (RCN) is acknowledged by the authors as follows: KWBH, LPC, KDK, JOF and HNB - FRIPRO Program (project number 250728); BP and JOF - Nano2021 (project number 250619); KDK and JOF - Petromaks2 (project number 280643); ECS, JOF and HNB - SYNKYT (project number 228551). KDK and JOF also acknowledge the financial support received from M-Era.Net (project number 272919) and ECS and HNB acknowledge support from The University of Copenhagen, The Niels Bohr Institute, the CoNexT project and the MAX4ESSFUN of the European Regional Development Fund Interreg Öresund-Kattegat-Skagerrak (project KU-019).

### Complementary information on authors:

Paulo H. Michels-Brito: [paulo.h.m.brito@ntnu.no](mailto:paulo.h.m.brito@ntnu.no) <https://orcid.org/0000-0002-6320-1171> [https://www.researchgate.net/profile/Paulo\\_Michels-Brito](https://www.researchgate.net/profile/Paulo_Michels-Brito)  
<https://www.linkedin.com/in/paulo-brito-b932a850/>  
<http://lattes.cnpq.br/9431456344824540>

Leander Michels: <a href="mailto:leander.michels@ntnu.no">leander.michels@ntnu.no</a> <a href="https://orcid.org/0000-0002-0023-681X">https://orcid.org/0000-0002-0023-681X</a> <a href="https://www.researchgate.net/profile/Leander_Michels">https://www.researchgate.net/profile/Leander_Michels</a> <a href="https://www.linkedin.com/in/leander-michels-a72316b4/">https://www.linkedin.com/in/leander-michels-a72316b4/</a> <a href="http://lattes.cnpq.br/4136579836712262">http://lattes.cnpq.br/4136579836712262</a>
Kristoffer W. B. Hunvik: <a href="mailto:kristoffer.hunvik@ntnu.no">kristoffer.hunvik@ntnu.no</a> <a href="https://orcid.org/0000-0002-2684-6464">https://orcid.org/0000-0002-2684-6464</a> <a href="https://www.researchgate.net/profile/Kristoffer_Hunvik">https://www.researchgate.net/profile/Kristoffer_Hunvik</a> <a href="https://www.linkedin.com/in/kristoffer-hunvik-a8429669/">https://www.linkedin.com/in/kristoffer-hunvik-a8429669/</a> <a href="https://www.ntnu.edu/employees/kristoffer.hunvik">https://www.ntnu.edu/employees/kristoffer.hunvik</a>
Everton C. dos Santos: <a href="mailto:ecsantos3013@gmail.com">ecsantos3013@gmail.com</a> <a href="https://orcid.org/0000-0002-1102-1101">https://orcid.org/0000-0002-1102-1101</a> <a href="https://www.researchgate.net/profile/Everton_Carvalho_Dos_Santos3">https://www.researchgate.net/profile/Everton_Carvalho_Dos_Santos3</a> <a href="http://lattes.cnpq.br/3755348881453343">http://lattes.cnpq.br/3755348881453343</a>
Barbara Pacáková: <a href="mailto:barbara.pacakova@ntnu.no">barbara.pacakova@ntnu.no</a> <a href="https://orcid.org/0000-0002-0408-0058">https://orcid.org/0000-0002-0408-0058</a> <a href="http://www.researcherid.com/rid/B-1703-2013">http://www.researcherid.com/rid/B-1703-2013</a> <a href="https://www.researchgate.net/profile/Leide_Cavalcanti">https://www.researchgate.net/profile/Leide_Cavalcanti</a> <a href="https://www.linkedin.com/in/leidecavalcanti">https://www.linkedin.com/in/leidecavalcanti</a>
Leide P. Cavalcanti: <a href="mailto:leide.cavalcanti@gmail.com">leide.cavalcanti@gmail.com</a> <a href="https://orcid.org/0000-0002-0408-0058">https://orcid.org/0000-0002-0408-0058</a> <a href="http://www.researcherid.com/rid/B-1703-2013">http://www.researcherid.com/rid/B-1703-2013</a> <a href="https://www.researchgate.net/profile/Leide_Cavalcanti">https://www.researchgate.net/profile/Leide_Cavalcanti</a> <a href="https://www.linkedin.com/in/leidecavalcanti">https://www.linkedin.com/in/leidecavalcanti</a>
Kenneth D. Knudsen: <a href="mailto:kenneth.knudsen@ife.no">kenneth.knudsen@ife.no</a> <a href="https://orcid.org/0000-0003-3091-2134">https://orcid.org/0000-0003-3091-2134</a> <a href="https://www.researchgate.net/profile/Kenneth_Knudsen">https://www.researchgate.net/profile/Kenneth_Knudsen</a> <a href="https://www.linkedin.com/in/kenneth-d-knudsen-6522ba99/">https://www.linkedin.com/in/kenneth-d-knudsen-6522ba99/</a>
Jon O. Fossum: <a href="mailto:jon.fossum@ntnu.no">jon.fossum@ntnu.no</a> <a href="https://orcid.org/0000-0002-8952-303X">https://orcid.org/0000-0002-8952-303X</a> <a href="https://publons.com/researcher/2235759/jon-o-fossum/">https://publons.com/researcher/2235759/jon-o-fossum/</a> <a href="http://folk.ntnu.no/fossumj/lab/people_jon.html">http://folk.ntnu.no/fossumj/lab/people_jon.html</a>
Heloisa N. Bordallo: <a href="mailto:bordallo@nbi.ku.dk">bordallo@nbi.ku.dk</a> <a href="https://orcid.org/0000-0003-0750-0553">https://orcid.org/0000-0003-0750-0553</a> <a href="https://www.researchgate.net/profile/Heloisa_Bordallo">https://www.researchgate.net/profile/Heloisa_Bordallo</a> <a href="https://dk.linkedin.com/in/heloisa-bordallo-92323a50/">https://dk.linkedin.com/in/heloisa-bordallo-92323a50/</a> <a href="https://xns.nbi.ku.dk/research/dynamics/">https://xns.nbi.ku.dk/research/dynamics/</a>

## REFERENCES

1. S.B. Hendricks, Zeitschrift für Kristallographie, vol. **959**, p 247 [1936]
2. H. H. Murray, Appl Clay Sci., vol. **17**, p. 207 [2000]
3. D. A. Laird, C. Shang, Clays Clay Miner., vol. **45**, p. 681 [1997]
4. D. L. Sparks, in *Environmental Soil Chemistry*, Academic Press Inc, UK [1995]
5. S. Rosenfeldt, M. Stöter, M. Schlenk, T. Martin, R. Q. Albuquerque, S. Förster, J. Breu, Langmuir, vol. **32**, p 10582 [2016]
6. S. Mukherjee, *The Science of Clays, Applications in Industry, Engineering, and Environment*, Springer Verlag, Germany [2013]
7. E. Eslinger and D. Pevear, in *Clay Minerals for Petroleum Geologists and Engineers*, SEPM Short Course Notes n° **22**, ix + 405 pp. Society of Economic

- Paleontologists and Mineralogists, Tulsa [1988].
8. F. Bergaya, G. Lagaly, M. Vayer, *Cation and Anion Exchange, in Handbook of Clay Science*, Elsevier, The Netherlands [2013]
  9. L. Delavernhe, M. Pilavtepe, K. Emmerich, *Appl Clay Sci.*, vol. **151**, p 175 [2018]
  10. M. Stöter, D. Kunz, M. Schmidt, D. Hirsemann, H. Kalo, B. Putz, J. Senker, J. Breu, *Langmuir*, vol. **29**, p1280 [2013]
  11. D. Carroll, *Geol Soc Am Bull.*, vol. **70**, p. 749 [1959]
  12. H. Kalo, W. Milius, J. Breu, *RSC Advances*, vol. **2**, 8452 [2012]
  13. H Li, T Kang, B Zhang, J Zhang, J. Ren, *Comput. Mater. Sci.*, vol **117**, p 33 [2016]
  14. K. M. Dontsova, L. D. Norton, C. T. Johnston, J. M. Bigham, *Soil Sci. Soc. Am. J.*, vol **68**, p 1218 [2004]
  15. J.M. Cases, I. Berend, M. Francois, J.P. Uriot, L.J. Michot, F. Thomas, *Clays Clay Miner.*, vol. **45**, p 8 [1997]
  16. J. Breu, W. Seidl, A. J. Stoll, K. G. Lange, T. U. Probst, *Chem. Mater.*, vol. **13**, p 4213 [2001]
  17. M. Daab, N. J. Eichstaedt, C. Habel, S. Rosenfeldt, H. Kalo, H. Schießling, S. Förster, J. Breu, *Langmuir*, vol. **34**, p 8215 [2018]
  18. G. J. da Silva, J. O. Fossum, E. DiMasi, K. J. Maloy, S. B. Lutnaes, *Phys. Rev. E*, vol. **66**, p 011303 [2002]
  19. M. Ziadeh, B. Chwalka, H. Kalo, M. R. Schutz And J. Breu, *Clay Minerals*, vol. **47**, p 341 [2012]
  20. B. Dazas, B. Lanson, J. Breu, J.-L. Robert, M. Pelletier, E. Ferrage, *Micropor. Mesopor. Mat.*, vol. **181**, p 233 [2013]
  21. M. Jaber, S. Komarneni, C.H. Zhou, *Synthesis of Clay Minerals*, in *Handbook of Clay Science*, Elsevier, The Netherlands, p 223 [2013]
  22. B. Ruzicka, E. Zaccarelli, *Soft Matter*, vol. **7**, p 1268 [2011]
  23. N.I. Ringdal, D.M. Fonseca, E.L. Hansen, H. Hemmen & J.O. Fossum *Phys. Rev. E* vol. **81**, p 041702 [2010]
  24. H. Hemmen, N. I. Ringdal, E. N. De Azevedo, M. Engelsberg, E. L. Hansen, Y. Meheust, J. O. Fossum, K. D. Knudsen, *Langmuir*, vol. **25**, p 12507 [2009]
  25. E. L. Hansen, H. Hemmen, D. M. Fonseca, C. Coutant, K. D. Knudsen, T. S. Plivelic, D. Bonn, J. O. Fossum, *Sci. Rep.*, vol. **2**, p 618 [2012],
  26. D.M.Fonseca, Y. Meheust, J.O. Fossum, K.D. Knudsen, K.P.S. Parmar, *Phys.Rev.E*, vol. **79**, p 021402 [2009]
  27. H Kalo, MW Möller, M Ziadeh, D Dolejš, J Breu, *Appl Clay Sci*, vol. **48**, p 39 [2010]
  28. M. W. Möller, T. Lunkenbein, H. Kalo, M. Schieder, D. A. Kunz, J. Breu, *Adv. Mater.*, vol. **22**, p 5245 [2010]
  29. H. Kalo, M. W. Möller, D. A. Kunz, J. Breu, *Nanoscale*, vol. **4**, p 5633 [2012]

30. M.A.S. Altoé, L. Michels, E.C.d. Santos, R. Droppa Jr, G. Grassi, L. Ribeiro, K.D. Knudsen, H.N. Bordallo, J.O. Fossum, G.J. da Silva, *Appl. Clay Sci.*, vol. **123**, p 83 [2016]
31. R. P. Tenorio, M. Engelsberg, J. O. Fossum, G. J. da Silva, *Langmuir*, vol. **26**, p 9703 [2010]
32. H. Hemmen, L. R. Alme, J. O. Fossum, Y. Meheust, *Phys. Rev.*, vol. **82**, p 036315 [2010]
33. R. P. Tenorio, L. R. Alme, M. Engelsberg, J. O. Fossum, F. Hallwass, *J. Phys. Chem. C*, vol. **112**, p 575 [2008]
34. L. Michels, Y. Méheust, M. A. Altoé, É. C. dos Santos, H. Hemmen, R. Droppa Jr, J. O. Fossum, G. J. da Silva, *Phys. Rev. E*, vol. **99**, p 013102 [2019]
35. L. Michels, L. Ribeiro, M. S. Pedrosa Mundim, M. H. Sousa, R. Droppa, Jr., J. O. Fossum, G. J. da Silva, K. C. Mundim, *Appl. Clay Sci.*, vol. **96**, p 60 [2014]
36. E. Ferrage, *Clay Clay Miner.*, vol. **64**, p 348 [2016]
37. B. Dazas, B. Lanson, A. Delville, J. L. Robert, S. Komarneni, L. J. Michot, E. Ferrage, *J. Phys. Chem. C*, vol. **119**, p 4158 [2015]
38. F. Salles, O. Bildstein, J. Douillard, M. Jullien, J. Raynal, H. Van Damme, *Langmuir*, vol. **26**, p 5028 [2010]
39. K. D. Knudsen, J. O. Fossum, G. Helgesen, M. W. Haakestad, *Physica B*, vol. **352**, p 247 [2004]
40. K. D. Knudsen, J. O. Fossum, G. Helgesen, V. Bergaplass, *J. Appl. Crystallogr.*, vol. **36**, p 587 [2003]
41. M. L. Martins, W.P. Gates, L. Michot, E. Ferrage, V. Marry and H.N. Bordallo, *Appl Clay Sci.*, vol. **96**, p 22 [2014]
42. M. Stöter, D. A. Kunz, M. Schmidt, D. Hirsemann, H. Kalo, B. Putz, J. r. Senker, J. Brey, *Langmuir*, vol. **29**, p 1280 [2013]
43. N. Skipper, A. Soper, and M. Smalley, *J. Phys. Chem.*, vol. **98**, p 942 [1994]
44. T. J. Tambach, P. G. Bolhuis, E. J. Hensen, B. Smit, *Langmuir*, vol. **22**, p 1223 [2006]
45. T. J. Tambach, E. J. M. Hensen, B. Smit, *J. Phys. Chem. B*, vol. **108**, p 7586 [2004]
46. M. Benhamou, *OAJ Materials and Devices*, vol **3**, p 0730 [2018] - DOI: 10.23647/ca.md20180730
47. J. Fossum, Y. Méheust, K. Parmar, K. Knudsen, K. Måløy, D. Fonseca, *EPL*, vol. **74**, p 438 [2006]
48. C. Pitteloud, D.H. Powell, H.E. Fischer, *Phys. Chem. Chem. Phys.*, vol. **3**, p 556 [2001]
49. G. Tiwari, R. Tiwari, S. Bannerjee, L. Bhati, S. Pandey, P. Pandey, B. Sriwastawa, *Int. J. Pharm. Investig.*, vol. **2**, p 2 [2012]
50. H. C. Ansel, N. G. Popovich, L. V. Allen, in *Ansel's Pharmaceutical Dosage Forms and Drug Delivery Systems*, 6th ed., Lippincott Williams & Wilkins [2011]

51. K. Park, *J. Control. Release*, vol. **190**, p 3 [2014]
52. A. Rivera, L. Valdés, J. Jiménez, I. Pérez, A. Lam, E. Altshuler, L. C. De Ménorval, J. O. Fossum, E. L. Hansen, Z. Rozynek, *Appl. Clay Sci.*, vol. **124–125**, p 150 [2016]
53. F. E. K. Okaikue-Woodi, S. E. Kelch, M. P. Schmidt, C. E. Martinez, R. E. Youngman, L. Aristilde, *J. Colloid Interface Sci.*, vol. **513**, p 367 [2018]
54. P. Komadel, J. Madejova, M. Janek, W. P. Gates, R. J. Kirkpatrick, J. W. Stucki, *Clays Clay Miner.*, vol. **44**, p 228 [1996]
55. P. Komadel, J. Madejová, *Dev. Clay Sci.*, vol. **1**, p 263 [2006]
56. E. C. dos Santos, W. P. Gates, L. Michels, F. Juranyi, A. Mikkelsen, G. J. Silva, J. O. Fossum, H. N. Bordallo, *Appl. Clay Sci.*, vol. **166**, p 288 [2018]
57. L. Valdés, D. Hernández, L. C. de Ménorval, I. Pérez, E. Altshuler, J. O. Fossum, A. Rivera, *Eur. Phys. J. Spec. Top.*, vol. **225**, p 767 [2016]
58. E. C. dos Santos, Z. Rozynek, E. L. L. Hansen, R. Hartmann-Petersen, R. N. N. Klitgaard, A. Løbner-Olesen, L. Michels, A. Mikkelsen, T. S. S. Plivelic, H. N. N. Bordallo, J. O. O. Fossum, *RSC Adv.*, vol. **7**, p 26537 [2017]
59. L. Valdés, I. Pérez, L. C. de Ménorval, E. Altshuler, J. O. Fossum, A. Rivera, *PLoS One*, vol. **12**, p e0187879 [2017]
60. D. Hernández, L. Lazo, L. Valdés, L. C. de Ménorval, Z. Rozynek, A. Rivera, *Appl. Clay Sci.*, vol. **161**, p 395 [2018]
61. Symes, W. S., Edwards, D. P., Miettinen, J., Rheindt, F. E., Carrasco, L. R. *Nat. Commun.*, vol. **9**, p 4052 [2018]
62. *Intergovernmental Panel on Climate Change, 2018: Global warming of 1.5 °C, in an IPCC Special Report on the impacts of global warming of 1.5°C above pre-industrial levels and related global greenhouse gas emission pathways, in the context of strengthening the global response to the threat of climate change, sustainable development, and efforts to eradicate poverty*, Editors V. Masson-Delmotte, P. Zhai, H.-O. Pörtner, D. Roberts, J. Skea, P.R. Shukla, A. Pirani, W. Moufouma-Okia, C. Péan, R. Pidcock, S. Connors, J.B.R. Matthews, Y. Chen, X. Zhou, M.I. Gomis, E. Lonnoy, T. Maycock, M. Tignor, T. Waterfield, *In press*
63. D. W. Dockery, C. A. Pope, X. Xu, J. D. Spengler, J. H. Ware, M. E. Fay, B. G. Ferris Jr, F. E. Speizer, *N. Engl. J. Med.* vol. **329**, p. 1753 [1993]
64. J. Fischer, R. Dyball, I. Fazey, C. Gross, S. Dovers, P. R. Ehrlich, R. J. Brulle, C. Christensen, R. J. Borden, *Front. Ecol. Environ.* vol. **10**, p 153 [2012]
65. Y. Zeng, R. Zou, Y. Zhao, *Adv. Mater.*, vol. **28**, p 2855 [2016]
66. D. Li, H. Furukawa, H. Deng, C. Liu, O. M. Yaghi, D. S. Eisenberg, *Proc. Natl. Acad. Sci.*, vol. **111**, p 191 [2014]
67. C. Gebald, J. A. Wurzbacher, P. Tingaut, T. Zimmermann, A. Steinfeld, *Environ. Sci. Technol.*, vol. **45**, p 9101 [2011]
68. S. J. Rukmani, T. P. Liyana-arachchi, K. E. Hart, C. M. Colina, *Langmuir*, vol. **34**, p. 3949 [2018]

69. J. Liu, X. Liu, Y. Sun, C. Sun, H. Liu, L. A. Stevens, K. Li, C. E. Snape, Adv. Sustain. Syst., vol. **2**, p. 1700115 [2018]
70. Y. Ren, R. Ding, H. Yue, S. Tang, C. Liu, J. Zhao, W. Lin, B. Liang, Appl. Energy, vol. **198**, p 250 [2017]
71. L. P. Cavalcanti, G. N. Kalantzopoulos, J. Eckert, K. D. Knudsen, and J. O. Fossum, Sci. Rep., vol. **8**, p. 11827 [2018]
72. L. Michels, J. O. Fossum, Z. Rozynek, H. Hemmen, K. Rustenberg, P. A. Sobas, G. J. da Silva, Sci. Rep., vol. **5**, p. 8775 [2015]
73. A. Chakraborty, A. Achari, M. Eswaremoorthy, and T. K. Maji, Chem. Commun., vol. **52**, p 11378 [2016]
74. D. R. Cole, A. A. Chialvo, G. Rother, L. Vlcek, P. T Cummings, Philos. Mag. vol **90**, p 2339 [2010]
75. H. Furukawa, N. Ko, Y. Go, N. Aratani, S.B Choi, E. Choi, A.O. Yazaydin, R.Q. Snur, M. O'Keeffe, J. Kim, O. Yaghi, Science, vol. **329**, p 424 [2010]
76. K. Sumida, D. L. Rogow, J. A. Mason, T. M. McDonald, E. D. Bloch, Z. R. Herm T.-H. Bae, J. R. Long., Chem. Rev., vol. **112**, p 724 [2012]
77. M. Cox, R. Mokaya, Sustain. Energy Fuels, vol. **1**, p 1414 [2017]
78. S. Cavenati, C. A. Grande, A. E. Rodrigues, J. Chem. Eng. Data, vol. **49**, p 1095 [2004]
79. P. R. Jeon, J. Choi, T. S. Yun, C. H. Lee, Chem. Eng. J., vol. **255**, p 705 [2014]
80. A. Busch, S. Alles, Y. Gensterblum, D. Prinz, D. N. Dewhurst, M. D. Raven, H. Stanjek, B M. Krooss, Int. J. Greenh. Gas Control, vol. **2**, p 297 [2008]
81. Y. H. Chen, D. L. Lu, Appl. Clay Sci., vol. **104**, p 221 [2015]
82. A. A. Pribylov, S. Z. Muminov, I. A. Kalinnikova, L. G. Shekhovtsova, Colloid J., vol. **72**, p 417 [2010]
83. L. Stevens, K. Williams, W. Y. Han, T. Drage, C. Snape, J. Wood, J. Wang, Chem. Eng. J., vol. **215**, p 699 [2013]
84. V. N. Romanov, Int. J. Greenh. Gas Control, vol. **14**, p 220 [2013]
85. Q. Rao, Y. Leng, J. Phys. Chem. C, vol. **120**, p 2642 [2016]
86. H. T. Schaefer, J. S. Loring, V. A. Glezakou, Q. R. Miller, J. Chen, A. T. Owen, C. Thompson, Geochim. Cosmochim. Acta, vol. **161**, p 248 [2015]
87. H. Sun, H. Zhao, N. Qi, X. Qi, K. Zhang, Y. Li, Mol. Simul., vol. **43**, p 1004 [2017]
88. C. Volzone, J. O. Rinaldi, J. Ortiga, Mater. Res., vol. **5**, p 475 [2005]
89. W. Wang, J. Xiao, X. Wei, J. Ding, X. Wang, C. Song, Appl. Energy, vol. **113**, p 334 [2014]
90. E. A. Roth, S. Agarwal, R. K. Gupta, Energy and Fuels, vol. **27**, p 4129 [2013]
91. P. Sozzani, S. Bracco, A. Comotti, M. Mauri, R. Simonutti, P. Valsesia, Chem. Commun., vol. **18**, p 1921 [2006]
92. E. Vilarrasa-García, J. A. Cecilia, M. Bastos-Neto, C. L. Cavalcante, D. C. S. Azevedo, E. Rodríguez-Castellón, Appl. Surf. Sci., vol. **410**, p 315 [2017]
93. N. Loganathan, A. O. Yazaydin, R. J. Kirkpatrick, G. M. Bowers, J. Phys. Chem.

- C, vol **123**, p 4848 [2019]
94. H. T. Schaef, N. Loganathan, G. M. Bowers, R. J. Kirkpatrick, A. O. Yazaydin, S. D. Burton, K. M. Rosso, *ACS Appl. Mater. Interfaces*, vol. **9**, p 36783 [2017]
  95. N. Loganathan, G. M. Bowers, A. O. Yazaydin, H. T. Schaef, J. S. Loring, A. G. Kalinichev, R. J. Kirkpatrick, *J. Phys. Chem. C*, vol. **122**, p 4391 [2018]
  96. N. Loganathan, G. M. Bowers, A. O. Yazaydin, A. G. Kalinichev, R. J. Kirkpatrick, *J. Phys. Chem. C*, vol. **122**, p23460 [2018]
  97. D. M. Moore, R. C. Reynolds, *X-ray Diffraction and the Identification and Analysis of Clay Minerals*, Oxford University Press, UK [1997]
  98. E. Ferrage, B. Lanson, L. J. Michot, J-L. Robert. *J. Phys. Chem. C*, vol. **114**, p. 4515 (2010).
  99. J. Als-Nielsen, D. McMorrow. *Elements of Modern X-ray Physics*, 2nd Edition, Wiley, USA [2011]
  100. P. Thompson, D. Cox, J. Hastings, *J. Appl. Crystallogr*, vol. **20**, p 79 (1987).
  101. T. H. De Keijser, J. I. Langford, E. J. Mittemeijer, A. B. P. Vogels, *J. Appl. Crystallogr*. vol. **15**, p 308 (1982).
  102. G. Williamson, W. Hall, *Acta Metall.*, vol. **1**, p 22 [1953]
  103. G. L. Squires, *Introduction to the Theory of Thermal Neutron Scattering*, Third Edit.; Cambridge University Press, UK [1978]
  104. J. D. F. Ramsay, P. Lindner. *J. Chem. Soc. Faraday Trans.*, vol. **89**, p 4207 [1993]
  105. P. D. Kaviratna, T. J. Pinnavaia, P. A. Schroeder, *J. Phys. Chem. Solids*, vol **57**, p 1897 [1996]
  106. E. DiMasi, J.O. Fossum, T. Gog, C. Venkataraman, *Phys.Rev., E* vol. **64**, 061704 [2001]
  107. H. Hemmen, E. L. Hansen, N. I. Ringdal, J.O. Fossum, *Rev. cuba. fís. (Cuban J. of Phys.)*, vol. **29-1E**, p 59 [2012]
  108. C. V. Raman, K. S. Krishnan, *Nature*, vol. **121**, p 501 [1928]
  109. D. A. Long, *Raman spectroscopy*. McGraw-Hill, New York [1977]
  110. B. H. Stuart, *Infrared Spectroscopy: Fundamentals and Applications*, John Wiley and Sons, Ltd., West Sussex, vol. **8**, p 224 [2004]
  111. T. Kogure, Chapter 2.9 - *Electron Microscopy*, in *Developments in Clay Science*, Elsevier, The Netherlands [2013]
  112. S. Petit, Fourier Transform *Infrared Spectroscopy*, in *Handbook of Clay Science*, Bergaya F, Theng BKG, Lagaly G, 1st ed. Elsevier, p 909 [2006]
  113. J. Madejová, P. Komadel, *Clays Clay Miner.*, vol. **49**, p 410 [2001]
  114. B. B. Zviagina, D. K. Mccarty, J. Srodon, V. A. Drits, *Clays Clay Miner.*, vol. **52**, p 399 [2004]
  115. L. Vaculíková, E. Plevová, *Acta Geodyn Geomater*, vol. **2**, p 167 [2005]
  116. E. W. Maina, H. J. Wanyika, A. N. Gacanja, *Chem Mater Res.*, vol. **7**, p 43 [2015]

117. T. Kloprogge, Raman Spectroscopy of Clay Minerals, in *Develop. in Clay Sci.*, Elsevier, The Netherlands, vol. **8** p 150 [2017]
118. R. L. Frost, L. Rintoul, *Appl Clay Sci.*, vol. **11**, p 171 [1996]
119. M. Ritz, L. Vaculíková, J. Kupková, E. Plevová, L. Bartoňová, *Vib Spectrosc.*, vol. **84**, p 7 [2016]
120. M. F. Brigatti, E. Galán, B. K. G. Theng, *Dev Clay Sci.*, vol. **5** [2013]
121. A. Wang, J. J. Freeman, B. L. Jolliff, *J. Raman Spectrosc.*, vol. **46**, p 829 [2015]
122. M. Pelletier, L. Michot, B. Humbert, B. Odile, J. B. de Lacaillerie, J. L. Robert, *Am Mineral.*, vol. **88**, p 1801 [2003]
123. C. Rinaudo, M. Roz, V. Boero, M. Franchini-Angela, *Neues Jahrbuch für Mineralogie – Monatshefte*, vol. **2004**, p 537 [2004]
124. P. M. Dias, D. L. A. de Faria, V. R. L. Constantino, *J Incl Phenom Macrocycl Chem.*, vol. **38**, p 251 [2000]
125. S. S. Hou, F. L. Beyer, K. Schmidt-Rohr, *Solid State Nucl. Magn. Reson.*, vol. **22**, p. 110 [2002]
126. H. N. Bordallo, L. P. Aldridge, G. Jock Churchman, W. P. Gates, M.T. F. Telling, K. Kiefer, P. Fouquet, T. Seydel, Simon A. J. Kimber, *J. Phys. Chem. C*, vol. **112**, p 13982 [2008]
127. W. P. Gates, L. P. Aldridge, G. G. Guzman, R. A. Mole, D. Yu, G. N. Iles, A. Klapproth and H. N. Bordallo, *Appl Clay Sci.*, vol. **147**, p 97 [2017]
128. Y. Fukushima, T. Yamada, K. Tamura, K. Shibata, *Appl Clay Sci.*, vol. **155**, p 15 [2018]
129. V. Marry, E. Dubois, N. Malikova, S. Durand-Vidal, S. Longeville, J. Breu, *Environ. Sci. Technol.*, vol. **45**, p 2850 [2011]
130. C.P. Morrow, A. Ö. Yazaydin, M. Krishnan, G. M. Bowers, A. G. Kalinichev, R. J. Kirkpatrick, *J. Phys. Chem. C*, vol. **117**, p 5172 [2013]
131. D. Presti, A. Pedone, G. Mancini, C. Duce, M. R. Tiné, V. Barone, *Phys. Chem. Chem. Phys.*, vol. **18**, p. 2164 [2015]
132. A. Botan, B. Rotenberg, V. Marry, P. Turq, B. Noetinger *J. Phys. Chem. C*, vol. **114**, p 14962 [2010]
133. G. J. Kearley, *Spectrochim. Acta Part A Mol. Spectrosc.*, vol. **48**, p 349 [1992]
134. A. J. Ramirez-Cuesta, *Comput. Phys. Commun.*, vol. **157**, p 226 [2004]
135. R. T. Cygan, L. L. Daemen, A. G. Ilgen, J. L. Krumhansl, T. M. Nenoff, *J. Phys. Chem. C*, vol. **119**, p 28005 [2015]
136. A. Gerstmans, L. Urbanczyk, R. Jérôme, J. L. Robert, J. Grandjean, *Clay Miner.*, vol. **43**, p 205 [2008]
137. L. Huve, L. Delmotte, P. Martin, R. Le Dred, J. Baron, D. Saehr, *Clays Clay Miner.*, vol. **40**, p 186 [1992]
138. J.-R. Butruille, T. J. Pinnavaia, *Alumina pillared clays as alkylation catalysis, in Clays: Controlling the Environment*. Proc. 10th Int. Clay Conf. Adelaide - Australia, G. J. Churchman, R. W. Fitzpatrick, R. A. Eggleton, CSIRO Publishing, Melbourne, Australia [1995]

139. J. Hougardy, W. E. Stone, J. J. Fripiat, *J. Chem. Phys.*, vol. **64**, p. 3840 [1976]
140. T. Dabat, F. Hubert, E. Paineau, P. Launois, C. Laforest, B. Grégoire, B. Dazas, E. Tertre, A. Delville and E. Ferrage, *Nat. Commun.*, vol. **10**, p 1 [2019].
141. G. Xie, D. Huang, Y. Xiao, M. Deng and P. Luo, *ACS Sustainable Chem. Eng.*, vol **8**, p 10303 [2020].
142. D. Vinci, B. Dazas, E. Ferrage, M. Lanson, V. Magnin, N. Findling and B. Lanson, *Appl Clay Sci.*, vol. **184**, p105404 [2020]
143. A. Aguiar, L. Michels, F. da Silva, C. Kern, G. Gomide, C. Ferreira, J. Depeyrot, R. Aquino and G. da Silva, *Appl Clay Sci.*, vol. **193**, p 105663 [2020]
144. P. Loch, K. W. B. Hunvik, F. Puchtler, S. Weiß, K. K. Seljelid, P. M. Røren, S. Rudic, S. Raaen, K. D. Knudsen, H. N. Bordallo, J. O. Fossum and J. Breu, *Appl Clay Sci.*, vol. **198**, p 105831 [2020]
145. S. R. Larsen, L. Michels, É. C. dos Santos, M. C. Berg, W. P. Gates, L. P. Aldridge, T. Seydel, J. Ollivier, M. T. F. Telling, J. O. Fossum and H. N. Bordallo, *Micropor. Mesopor. Mat.*, vol. **306**, p 110512 [2020]
146. C. Hiebl, P. Loch, M. Brinek, M. Gombotz, B. Gadermaier, P. Heitjans, J. Breu and H. M. R. Wilkening, *Chem. Mater.*, vol. **32**, p 7445 [2020]
147. L. Michels, C. L. S. da Fonseca, Y. Méheust, M. A. S. Altoé, E. C. dos Santos, G. Grassi, R. Droppa Jr., K. D. Knudsen, L. P. Cavalcanti, K. W. B. Hunvik, J. O. Fossum, G. J. da Silva, and H. N. Bordallo. *J. Phys. Chem. C*, vol. **124**, p 24690 [2020]